metals

Article

Numerical and Experimental Studies on the Load Characteristics of Geometric Interference of Steel-Aluminum Knurled Interference Fit

Chi-Peng Chen, Marlon Ho, Tomi-T. Li and Yiin-Kuen Fuh *

Department of Mechanical Engineering, National Central University, Taoyuan County 32001, Taiwan
* Correspondence: michaelfuh@gmail.com

Abstract: This research studied the knurled interference fits (KIF) jointing process, which involves connection via a shaft and hub. KIF are widely used in many industries and products, but the related research is limited, especially in the case of auto parts. To confirm the optimal parameters for KIF joining, two different simulations in the finite element method (FEM), two hub thicknesses, three geometry versions, and four coefficients of friction (COF) were adopted to simulate the KIF forming process in this study. All the parameters were investigated in detail and accurately referred to experimental examination outcomes. The simulations and the experimental results offered explicit explanations of the relationship between jointing force and geometry dimensions. The hub-forming shape and the simulation of hoop deformation were analyzed, and the analysis results provide useful suggestions for other related industrial research as well.

Keywords: finite element method (FEM); knurled interference fits (KIF); gear jointing force; symmetric segment simulation method; assembling deformation

check for updates

Citation: Chen, C.-P.; Ho, M.; Li, T.-T.; Fuh, Y.-K. Numerical and Experimental Studies on the Load Characteristics of Geometric Interference of Steel-Aluminum Knurled Interference Fit. *Metals* **2022**, *12*, 2078. https://doi.org/10.3390/met12122078

Academic Editors: Antonio Mateo and Giovanni Meneghetti

Received: 1 November 2022
Accepted: 1 December 2022
Published: 3 December 2022

Publisher's Note: MDPI stays neutral with regard to jurisdictional claims in published maps and institutional affiliations.

Copyright: © 2022 by the authors. Licensee MDPI, Basel, Switzerland. This article is an open access article distributed under the terms and conditions of the Creative Commons Attribution (CC BY) license (https://creativecommons.org/licenses/by/4.0/).

1. Introduction

Aluminum alloy materials have excellent wear resistance, corrosion resistance, and processability, and they have been widely used in various mechanical parts for manufacturing processes [1]. Many manufacturing industries often choose aluminum 6061 alloys as the workpiece to ensure the high quality, light weight, high fatigue life, and reliability of the workpiece [2]. Interference fits are often used in various engineering applications, such as the machinery industry and the automotive industry [3]. Many factors affect the bearing capacity of interference fits, such as the roundness of the void, the cylindricity, and the roughness of the contact surface [4]. Sohrabpoor et al. [5] used 316 L stainless steel to conduct interference fit experiments to study the effect of micro-surface texture (including shape and size) on the bonding strength and found that the height and size of the surface structure was the most critical factor affecting the bonding strength. For the surface of the shape design, the interference fit engagement force of the trapezoid is greater than that of oval and triangular designs. Lü et al. [6] studied how the fatigue life of composite bolted joints was affected by interference fit. The experimental range of the bolt interference fit was 0~1%, and the surface damage was observed by a scanning electron microscope (SEM). The experimental results showed that the fatigue life of the specimen using the interference fit was improved, and the degree of surface damage was better than that of the traditional fitting specimen. Romanov et al. [7] studied the assembly process of steel, titanium, and other materials and proposed a workpiece control assembly system to adjust the pressing speed, force, and stroke distance to ensure the assembly quality and stability of the connector. The experimental results confirmed the high accuracy of the developed control system. Obeidi et al. [8] used lasers to study surface textures for applications where mechanical components can be precisely controlled. Laser processing parameters were developed to optimize the material surface outer diameter and texture shape in order to analyze the key factors influencing interference fit parts. A predictable and repeatable novel surface texture was proposed for interference fit parts that can be used in many industries. Hirot et al. [9] studied the mechanical connection process of the shaft and the hole plate, used the knurled shaft to increase the axial strength of the interference fit, and analyzed the influence of the indentation depth of the workpiece surface on the joint force. In addition, using the interference fit for push-out and press-in experiments confirmed the torsional strength and connection strength of the joint. The forming and rotating locking method was better than those of the traditional spline modes. McMillan et al. [10] studied the effect of the pressure and friction coefficient of interference fit components on torque capacity. The experimental results of steel materials showed that the correlation between pressure and torque capacity at the workpiece interface was not significantly high, but the friction coefficient was important for increasing or maintaining torque. These results provide an important reference for optimizing the design of the interference fit. Most of the above research on shaft-hole interference fits only studied the issues of jointing force and fatigue life, including the influence of shaft hole shape and size on joint strength, the fatigue life of bolted joints, and the surface texture by using laser design and jointing method differences. Relatedly, none of the studies have conducted additional research on the influence of deformation on the interference fit, which is also one of the items that this study aimed to explore in depth.

The finite element method has a reference value for research and analysis of mechanical and industrial design [11,12], and this method is often used to analyze the degree of correlation between related influencing factors. A finite element method is a tool that can analyze uncertainty factors [13]. Lou et al. [14] used the finite element method (FEM) to analyze the part assembly procedure of precision interference fit and studied the influence of the error of part positioning and displacement measurement on assembly accuracy. Using the force-displacement curve to evaluate the quality of the assembly, they proposed a new assembly calibration method and obtained precise experimental results regarding the assembly, with minimal deviation of the position and parallelism of the parts. Wang et al. [15] used the finite element method (FEM) to analyze the assembly process of interference fit parts and proposed a new simplified model to calculate the resistance value of the press fit process. The experimental results verified that the new calculation method could replace the traditional thick-walled cylinder and accurately predict the interference fit curve values in the theoretical press-fit curve. Zhang et al. [16] used finite element simulation combined with the response surface method (RSM) to analyze the radial connection process of the wheel and axle. The relevant factors influencing the results included gear height, gear angle, and press-fit feed. The experimental results showed that the gear that adopts the knurled design can improve the torsional strength of the assembly, and a set of optimized design parameters was proposed. The model provided an important reference value for research regarding the knurled connection. Lanoue et al. [17] used the finite element method to analyze interference fit components to determine the optimal design parameters of the interference fit. Four different contact calculation methods were used to explore the assembly accuracy and manufacturing process of the press-fitting process. It was found that the contact stiffness and elastic slip of the workpiece were the main factors that affect the parameters of the optimal pressing process, and the optimal control parameters that could improve fatigue life were also proposed. Izard et al. [18] carried out numerical simulations of various bearing assemblies using the finite element method (FEM) with different geometries and material designs to improve the problem of workpiece stress concentration. It was found that the thickness of the hub greatly influenced the stress concentration, and it was proposed that there is a high correlation between the stress and stiffness of the contact ring. Although FEM research related to interference fit has contributed to multiple great studies, such as those assessing assembly accuracy, simplifying model simulation, assessing gear shape, assessing angle, and studies of optimal process parameters, a single simulation method is usually used, and multiple simulation methods have not been compared and verified. Therefore, this study will conduct related research using more than two simulation methods and simplified models to improve the reliability and practicality of simulation modeling results.

This study aimed to confirm the optimal parameters for KIF joining using two different simulations utilizing the finite element method. Two hub thicknesses, three geometry versions, and four coefficients of friction (COF) were adopted to simulate the KIF forming process, and simulation results were verified by subsequent experiments. This study established a new symmetrical simulation method and performed comparisons. It conducted in-depth research on hoop (hole) deformation and gear formability, which are generally less researched. It is expected to improve the current problems of the jointing force and deformation of shaft hole fit. The results can provide some important reference information for related industries and research.

2. Methodology and Materials of the Experiment

2.1. Design Parameters and Jointing Process

The wheel hub is one of the crucial parts supporting the vehicle's drive axle. Its structural rigidity and structural life are important factors affecting the quality of the car, the assembly operation of the wheel hub, and the stability of the wheel axle structure.

This study analyzed the press-fit process between the shaft (punch) and the vehicle wheel hub, as shown in Figure 1a. The relevant wheel hub is often used in various vehicle structural systems, as illustrated in Figure 1b [19]. The knurled interference fits (KIF), which is the knurled area of the shaft (punch) to connect to the hub, and the dimensions of the shaft diameter were bigger than the inner dimension of the hub during the jointing process. The KIF is utilized to make a connection between the shaft and the hub during the process, as shown in Figure 1c. The shapes of the knurl profile of the workpiece, the dimensions at the surface, and the interior of the whole structure are shown in Figure 1d–f. These dimensions explain the direction, angle, and position of the knurls and the hub. Furthermore, the KIF and the knurled area design parameters of the shaft and hub are displayed below:

- KIF area diameter of shaft D_1;
- The height of shaft H_1;
- Shaft height of the other sections H_2, H_3, H_4;
- Shaft diameter D_2;
- Shaft chamfer angle φ;
- Outer diameter of hub D_{oH};
- Inner diameter of hub D_{iH};
- pitch t;
- Tooth height $H_{k.}$

The material of the hub was AA6061, the material of the shaft was ASTM-H13, and the materials' chemical compositions are listed in Tables 1 and 2. The working temperature of both the hub and the shaft was 20 degrees, the heat conduction coefficient was 0.3, and the Coulomb friction law was adopted. The setting parameters of the simulation and experiment of this study are shown in Table 3. The flow stress parameters of aluminum alloys usually depend on the thickness of the sheet [20]. To define the flow stress values (k_f) of material 6061 at different material thicknesses (so the software could receive the correct simulation results), the calculation Formulas (1) and (2) by Ludwik (1909) [21] were used to obtain an approximate value of the flow stress vs. true strain as illustrated in Figure 2. The true strain is the value of the area of the material changing when the material is deformed.

$$k_{f=C\times\varepsilon_v^n} \tag{1}$$

$$C = R_m \times \left(\frac{e}{n}\right)^n \tag{2}$$

where C in the formula describes the specific constant of the material, ε_v represents the equivalent plastic strain, R_m is the tensile strength of the material, e is Euler's number, and n is the strain hardening coefficient.

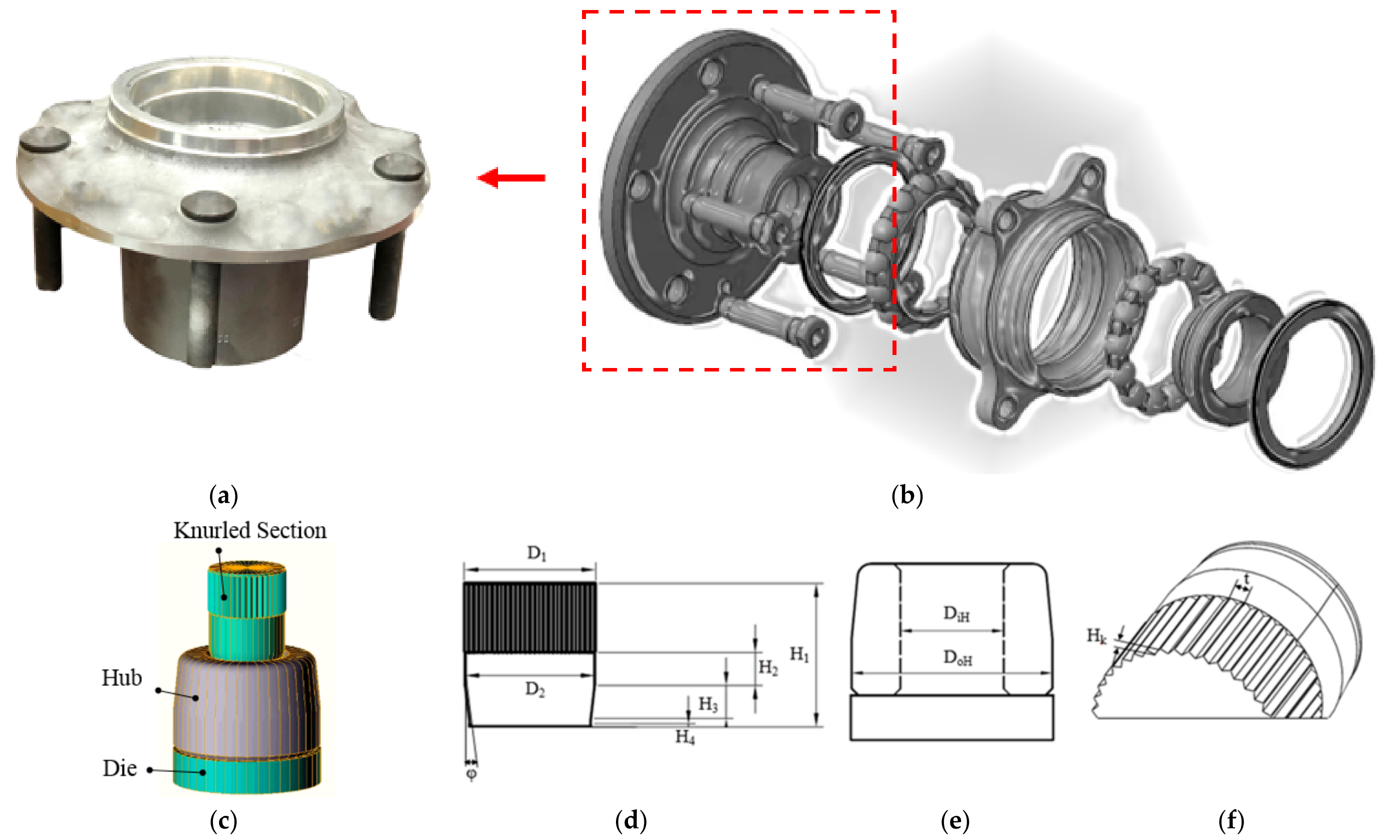

Figure 1. The main research items of this paper: (**a**) the workpiece of the hub structure, (**b**) the expanded view of the wheel structure, (**c**) 3D drawing of the structure, (**d**) the view of the shaft design dimensions, (**e**) the side view of the hub design dimensions, and (**f**) the design dimensions of the knurl area.

Table 1. Chemical composition of AA6061.

AA 6061 (wt%)	Al	Mg	Si	Cu	Mn	Fe	Cr	Zn
	>97.00	<0.90	<0.80	<0.30	<0.20	<0.40	<0.02	<0.18

Table 2. Chemical composition of ASTM-H13.

ASTM-H13 (wt%)	C	V	Si	Mn	P	S	Cr
	0.32–0.45	0.8–1.2	0.8–1.2	0.2–0.5	$0 \leq 0.03$	$0 \leq 0.03$	4.75–5.5

Table 3. The parameters of the forging process.

Hub Material	**AA6061**
Hub temperature	20 °C
Shaft material	ASTM-H13
Shaft temperature	20 °C
Coefficient of friction (COF)	0.45~0.8
Heat transfer coefficient	0.3
Environment temperature	20 °C
Element style	Tetrahedron
Mesh size of blank	1 mm
Mesh size of dies	1–16 mm
Contact definition	Frictional contact

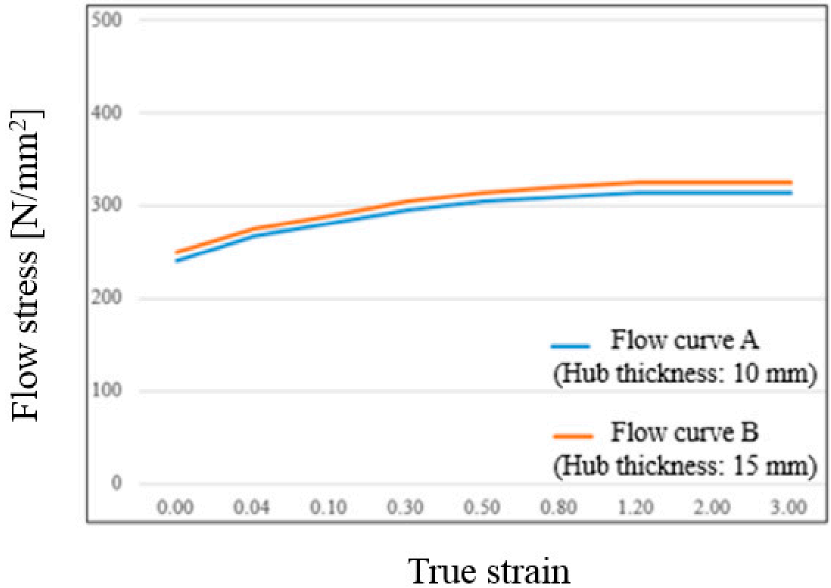

Figure 2. Flow curves of the different hub thicknesses for AA 6061.

2.2. Shaft Design and Dimensions of Hubs

To investigate the critical parameters that influence KIF details, three different numerical models were initially set up as shown in Figure 3a–c, the dimension differences between the figures are shown in red font. These models were established by the finite element software, QForm, (9.0.7, Oxford, UK) and the relative dimensions of the models were provided directly by the manufacturer. The crucial dimensions for the numerical simulations include the diameter of shaft D_1, shaft chamfer angles φ, dimensions of the hub, etc. The outer diameter of the shaft is bigger than the hub's inner dimension, which can cause a geometric interference phenomenon when the axial direction of the shaft eventually presses into the hub during the jointing process. Thus, the theoretically relative formula for geometric interference is shown in Equation (3) as follows:

$$\text{Geometric interference } I_{geo} = |D_{iH} - D_1| \tag{3}$$

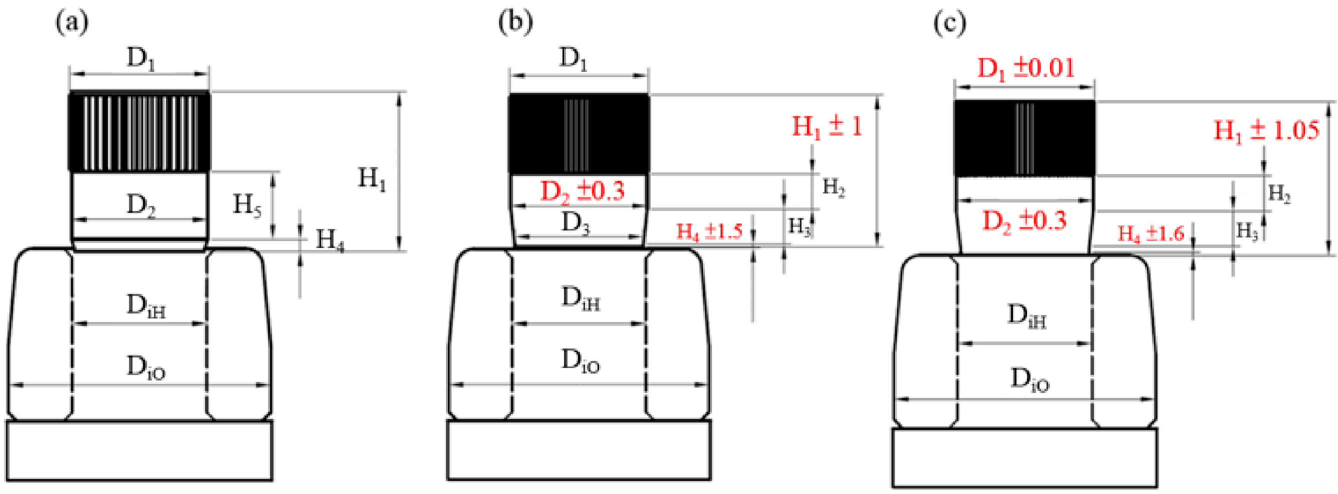

Figure 3. Different design versions of the shaft: (**a**) version 1, (**b**) version 2, and (**c**) version 3.

The main structure examined in this study is shown in Figure 4. It included the shaft (punch) and the hub, and the driving force slowly pushes the shaft to get into the hub to connect these two parts of the structure during the jointing process. The contact region between knurled section and the inner hub was the most important observation position for the research. Moreover, the dimension of the knurled section was quite small (height 0.17 mm). It needs to mesh the connection region very evenly in the FE software. Thus, the mesh was refined to 0.01 mm both in the KIF region and hub. To build a dimensional sketch, SolidWorks software (SP 1.0, premium, Waltham, MA, USA) was used to make up the entire workpiece, such as forming the shape design, pattern sketch, inside and outside diameter of the hub, forming tolerance, etc.

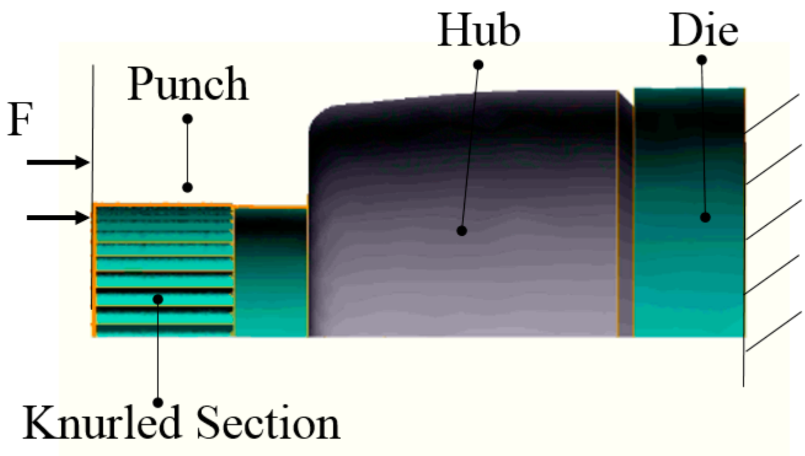

Figure 4. Setup of the jointing process.

The different shaft chamfer angles and the dimension of the shafts are shown in Figure 5a; version 1 had the largest chamfer angle (16.77°) and the shortest chamfer length. Figure 5b illustrates the chamfer dimensions (6.63°) of version 2 with the longest chamfer dimensions of the shaft. Figure 5c shows version 3, which had the same chamfer angle as version 2 and contained a moderate distance dimension of the shaft.

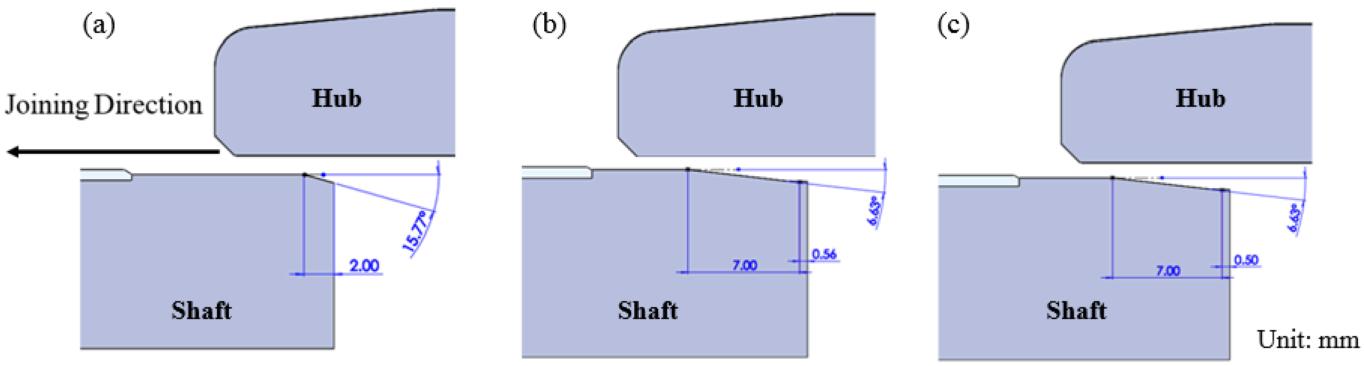

Figure 5. Different version of shaft dimensions: (**a**) version 1, (**b**) version 2, and (**c**) version 3.

3. Finite Element Method (FEM) Model and Experimental Validation

Because the mesh size of the contact region is very small, it is best to use the symmetric segment method to simulate these design models. This can greatly reduce the computing time for different kinds of simulations. Moreover, considering the accuracy of the simulation result, two kinds of methods were used to execute the symmetric simulations in the FEM software (9.0.7, QForm, Oxford, UK) in this study. Correlative structure models are illustrated in Figure 6. Method A executed the symmetric simulation in design models as shown in Figure 6a,b. On the other hand, method B took one of the hoops from the whole hub to make another symmetric numerical computation as shown in Figure 6c,d.

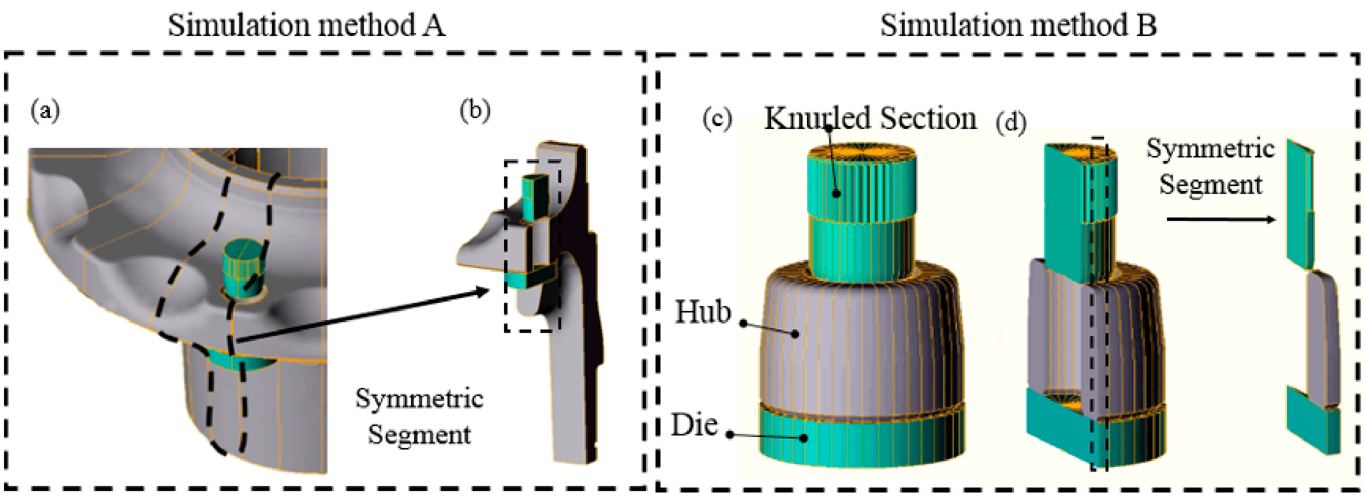

Figure 6. Design of simulation models: (**a**) one of knurled fit model, (**b**) symmetric segment of one knurled fit model, (**c**) one of a hoop of the hub, and (**d**) symmetric segment of a hoop.

Figure 7a shows a hydraulic drive device (which was used during the experiment) with 0.5 MN power to drive the punch to get into the hub [22]. Furthermore, Figure 7b illustrates the structure of the machine equipment. The machine structure, from top to bottom, consists of hydraulic equipment, upper die, push ram, lower die, and machine frame.

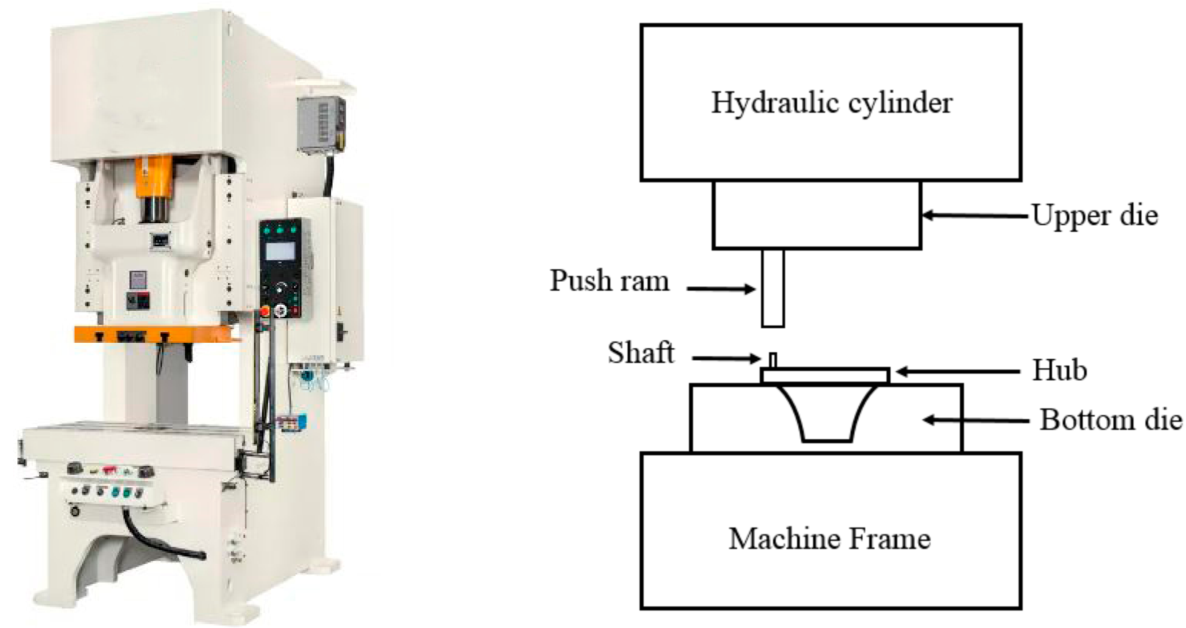

(**a**) (**b**)

Figure 7. Experimental equipment: (**a**) photo of machine used in experiments and (**b**) schematic of the machine.

The parameters of the study design are shown in Table 4. There were twelve parameter combinations that were designed. Simulations containing two different shaft chamfer angles, two kinds of shaft diameters, four different coefficients of friction (COF), and two hub thicknesses were modeled in the finite element software. Implementing these study values could help find the optimal experimental parameters for the jointing process.

Table 4. Parameters of the design for different tests.

Parameter	Version 1				Version 2				Version 3			
	Test No.											
	1	2	3	4	5	6	7	8	9	10	11	12
Shaft chamfer angle ϕ ($\circ$)	15.77				6.63							
Shaft diameter Ds (mm)	D1								D1 $\pm$ 0.01			
Geometric interference I_{geo} (mm)	0.2								0.2 $\pm$ 0.01			
Coefficient of friction (COF)	0.45	0.61	0.7	0.8	0.45	0.61	0.7	0.8	0.45	0.61	0.7	0.8
Hub thickness ($D_{io} - D_{iH}$)	10 mm & 15 mm											
Pitch t (mm)	1.8											
Joining length (mm)	26											

Comparison of the jointing force between the experiment and simulation with a hub thickness of 10 mm is shown in Figure 8a. F_j is the force value when the hub and shaft are engaged (the associated unit is KN). The experimental force values were drafted at the horizontal and the vertical axis as an inclined line in gray color. The values of the numerical computations are recorded on the y-axis of the diagram in Figure 8a, which shows the outcomes of the simulations with the experimental forces as a basis for comparison. Furthermore, deviation of the numerical data was represented on the graph as well. For those force values mentioned above, the maximum deviation of the joining force was +6.14% in method A, and the other values were both under $\pm$5%. On the other hand, the maximum deviation of the joining force was +4.86% in method B, and the others were both under ±5%. The results of these experiments and simulations, as assessed by comparing the mean results of the tests for both the experiments and simulations, were very similar and accurate.

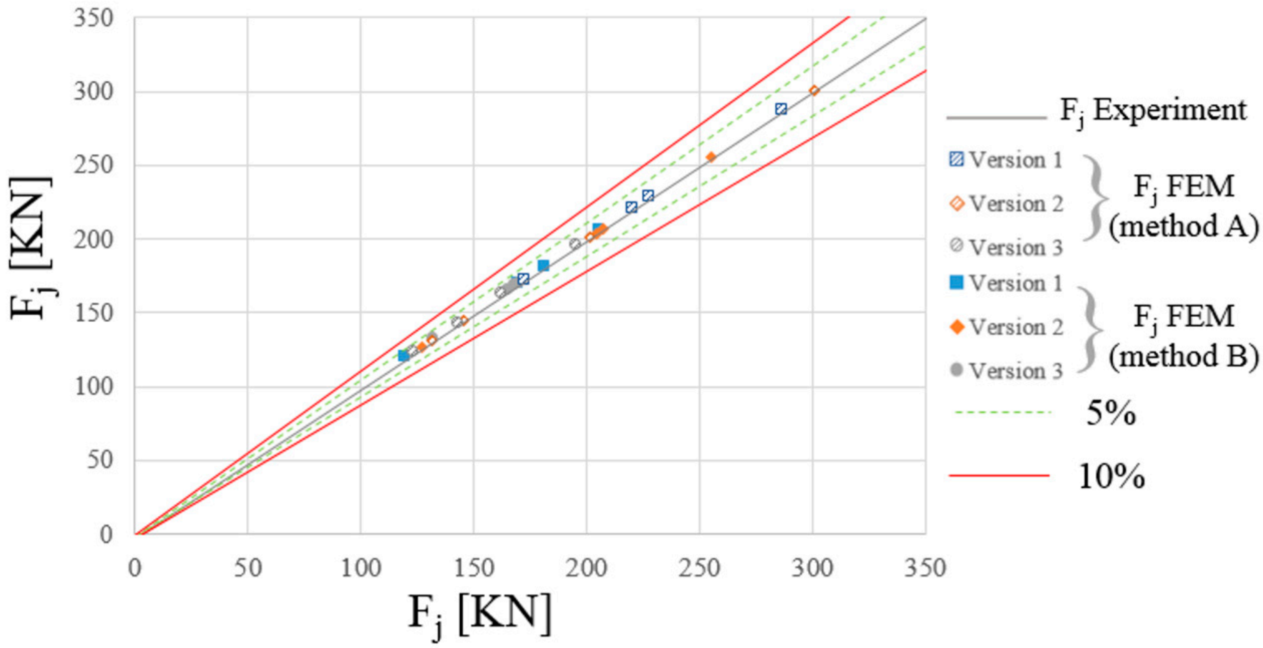

(**a**)

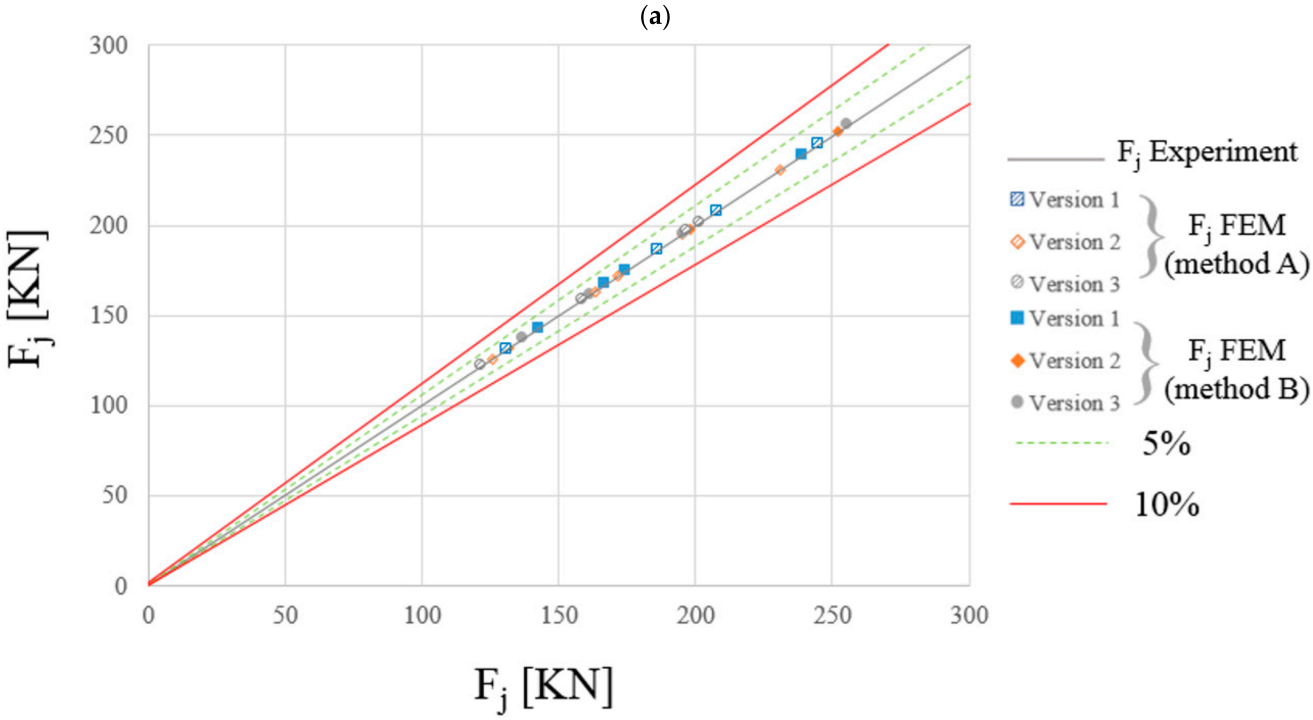

(**b**)

Figure 8. Comparison of the experimental and numerical forming process results with different hub thicknesses: (**a**) 10 mm and (**b**) 15 mm.

Comparison of the jointing force between the experiment and simulation with hub thicknesses of 15 mm is shown in Figure 8b. The experimental force values are shown at the horizontal and the vertical axis as an inclined line in gray color. The values of the numerical computations are recorded on the *y*-axis of the diagram in Figure 8a,b, which show the outcomes of the simulations with the experimental forces as a basis of comparison. The simulation and experimental results were similar to those of the hub thickness of 10 mm, and the numerical trend was also consistent. Moreover, the error values of the two methods were less than 5%, thus verifying the accuracy of the simulation analysis.

For the sake of understanding the jointing forces during the connection at the hubs, we used two kinds of numerical simulations (method A and method B) with experiments recorded the outcomes in Figure 9. F_j is the force value when the hub and shaft are engaged (the associated unit is KN). Sr is the experimental and simulated jointing force value. The relevant forming data are shown in Table 5.

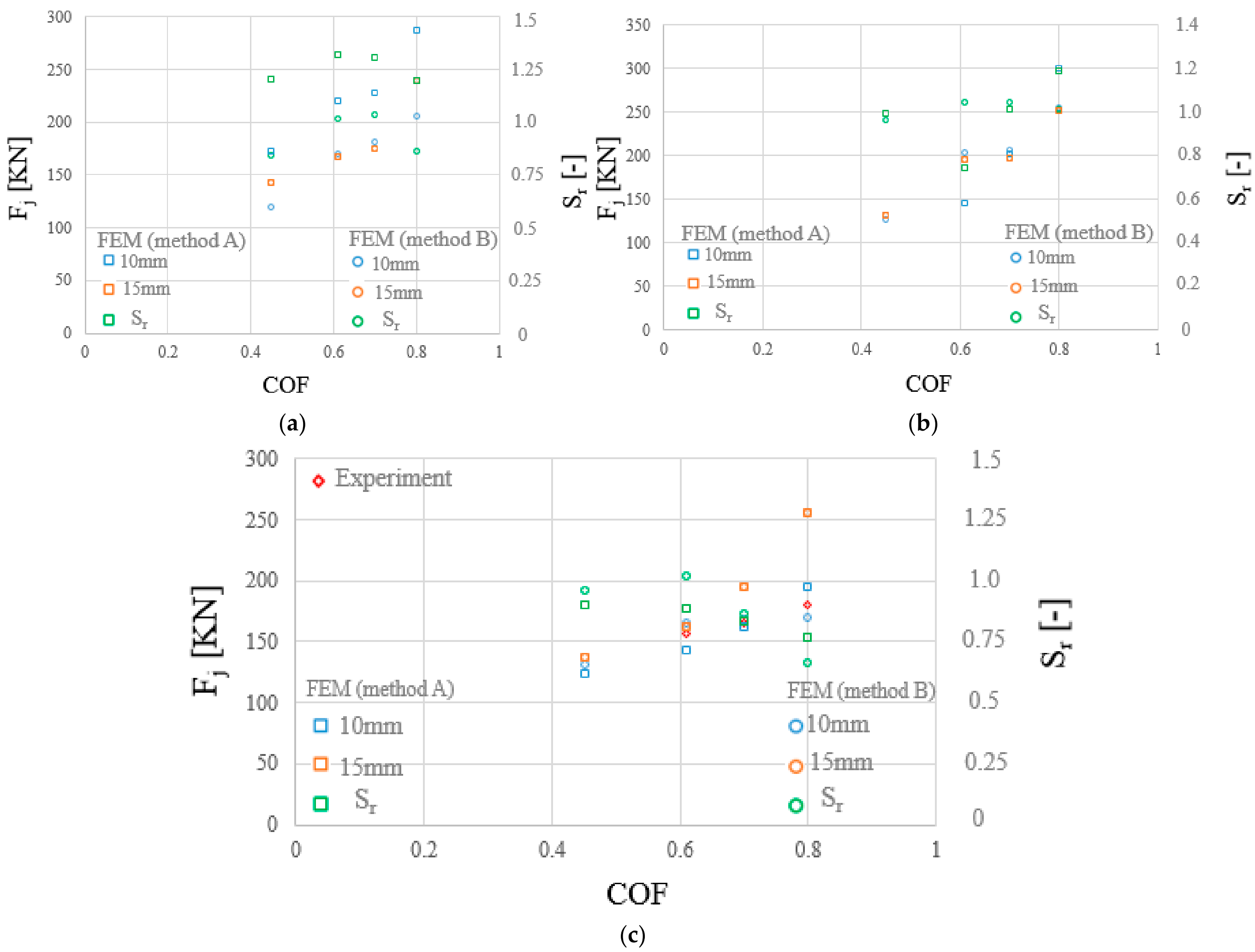

Figure 9. Joining force with different coefficients of friction (COF) in three geometries: (**a**) version 1, (**b**) version 2, and (**c**) version 3.

Table 5. Statistical table of bonding force data for different COFs in three versions of geometries.

	Hub Thickness	Simulation Method A	Mean Ratio of Joining Force Difference (FEM and Experiment)	Simulation Method B	Mean Ratio of Joining Force Difference (FEM and Experiment)
Version 1	10 mm	226.88 KN	78.63%	169.30 KN	95.76%
	15 mm	180.92 KN		180.93 KN	
Version 2	10 mm	194.61 KN	84.28%	198.25 KN	83.17%
	15 mm	194.27 KN		194.27 KN	
Version 3	10 mm	156.21 KN	97.72%	158.90 KN	96.91%
	15 mm	187.45 KN		187.45 KN	

According to the jointing force data in Table 5, the hub thickness had little influence on the experimental results of this study, and the related forming data were similar and had no single trend. Based on comprehensive analysis of all jointing force data, the version 3 shaft design had the lowest jointing force, and the data error between the simulation and the experiment was the smallest. Thus, version 3 appeared to be the best shaft design in this study.

If the jointing force of the jointing process is too high, manufacturers need to prepare large equipment and spend more money to conduct experiments. Therefore, according to the comparison of the jointing force data of the simulation and the experiment, the data error of simulation in method B was the smallest due to the mesh size being thinner than in method A. Thus, simulation method B should be the optimal simulation method for the KIF process. Finally, the jointing force was proportional to the COF value, as shown in Table 5, which means that COF is one of the crucial factors affecting the jointing force.

An enlarged view of the geometry of the contact area between the shaft and the hub was evaluated (as shown in Figure 10) to assess more details during an engagement for more relevant verification. According to the comparison of the deviation of hub size, the tooth profile similarity is extremely high between the experiment and simulation, which means that using the finite element model could allow more high-accuracy experimental analyses to be conducted in the future.

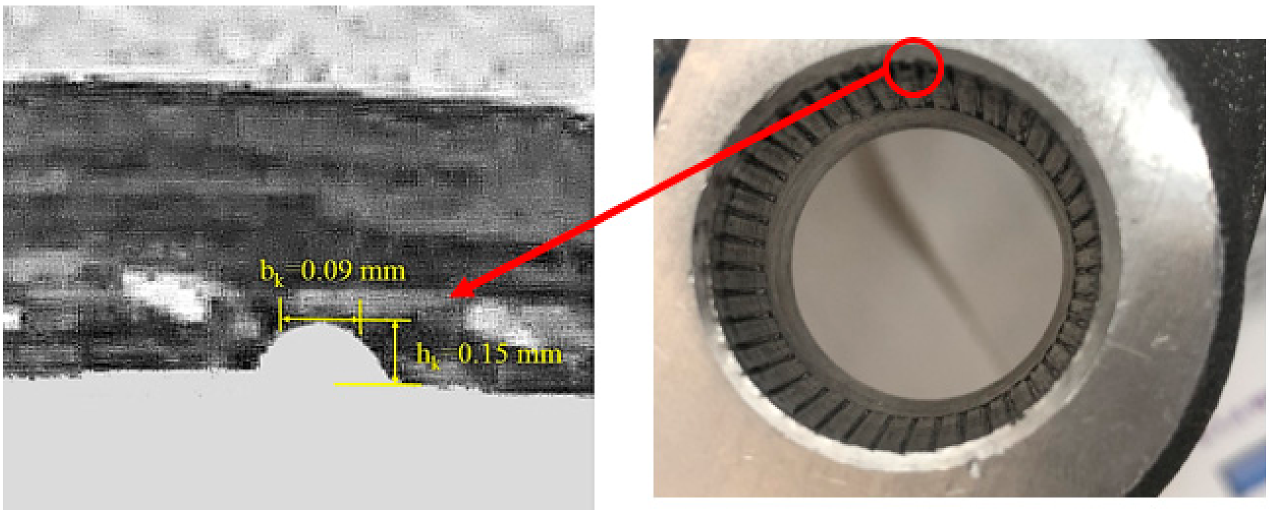

(**a**)

Figure 10. *Cont.*

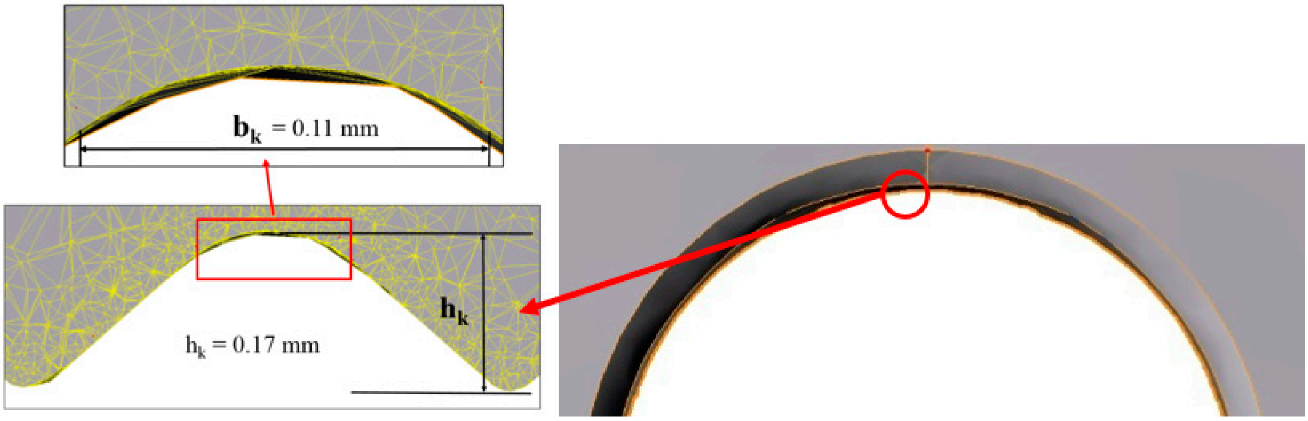

(**b**)

Figure 10. The contrast of experimental and numerical jointing process of the hub shape (version 3, COF 0.61): (**a**) optical photo of an experimental workpiece and (**b**) schematic simulation of workpiece.

Figure 11a shows simulation method A with a hub thickness of 10 mm. The average forming height (r) of the hub was 9.147 mm, and the ratio of the average height difference was 99.97%. Figure 11b shows the simulation method B with a hub thickness of 10 mm. The average forming height (r) of the hub was 9.128 mm, and the ratio of the average height difference was 99.98%. Figure 11c shows the simulation method A with a hub thickness of 15 mm. The average forming height (r) of the hub was 9.153 mm, and the ratio of the average height difference was 99.95%. Figure 11d shows the simulation method B with a hub thickness of 15 mm. The average forming height (r) of the hub was 9.127 mm, and the ratio of the average height difference was 99.98%.

According to the above analysis, simulation method B was more accurate than simulation method A. These figures show the formed shape of the hub after the shaft is connected to the hub. In the process of forming the connection, the hub has a small deformation. If the COF value is small, the horizontal expansion of the hub is larger. These larger expansions will result in less material flow in the contact area during the jointing process and reduce the knurl forming height at the hub. The result will be a reduction in axial strength and torsional loads in the process [20]. Therefore, according to the analysis results, to increase the binding force of KIF, the conditions with a large COF value should be selected for this study. However, if the COF value is too high, the joining force can easily become too large; thus, a moderate COF value should be selected.

Figure 12 shows the hoop deformations of version 3 hubs after executing the joint forming process. The optical photo and simulation figure of the hub are illustrated in Figure 12a,b. Numerical simulation results of the hoop by methods A and B with two kinds of hub thickness are shown in Tables 6 and 7. They indicate the hoop deformation dimensions during the joining process. In method A, the average deformation dimensions of the hoop hub with a thickness of 10 mm and 15 mm were 23.65 mm and 23.62 mm, respectively, and the ratios of deformation dimension differences with experimental values were both within 0.02%. Moreover, in method B, the average deformation dimensions of the hoop with a thickness of 10 mm and 15 mm were 23.74 mm and 23.50 mm, respectively, and the ratios of deformation dimension differences with experimental values were both within 0.04%. Therefore, the thickness of the hub and the simulation method have little effect on hoop deformation.

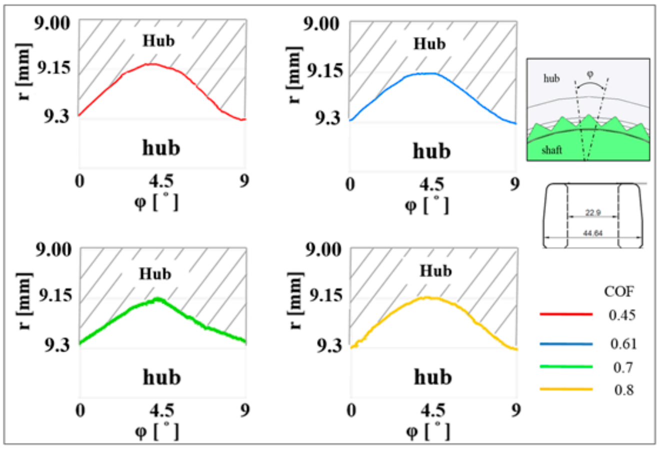

(**a**) Method A

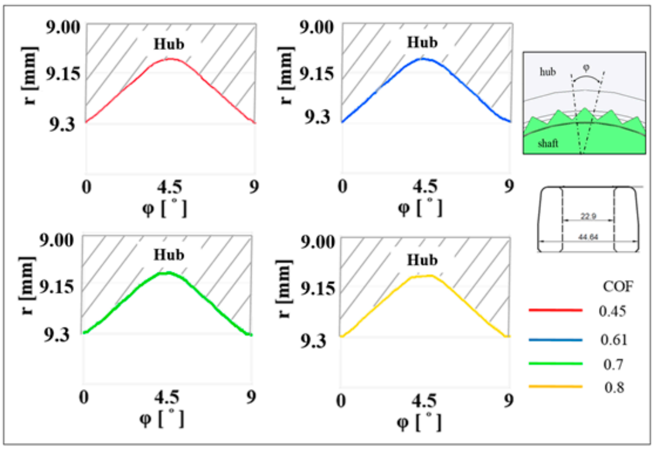

(**b**) Method B

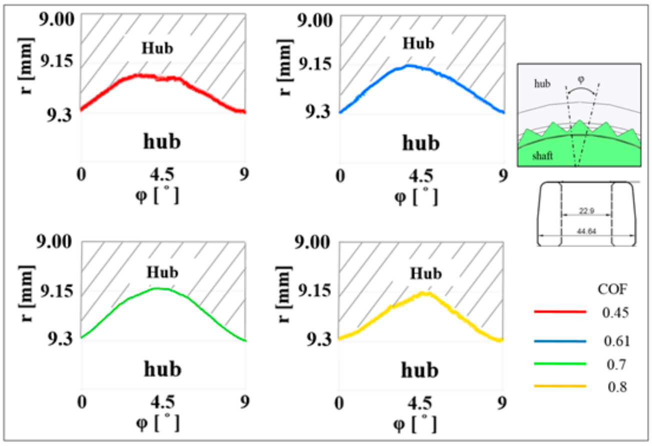

(**c**) Method A

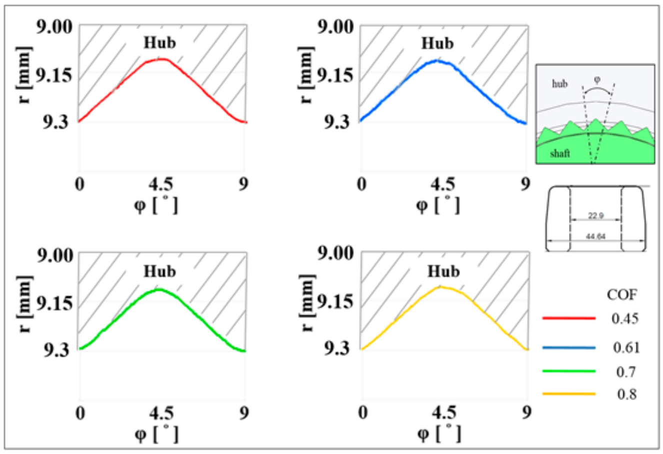

(**d**) Method B

Figure 11. Tooth profile comparison of version 3 hub: (**a**) hub thickness of 10 mm in method A, (**b**) hub thickness of 10 mm in method B, (**c**) hub thickness of 15 mm in method A, and (**d**) hub thickness of 15 mm in method B.

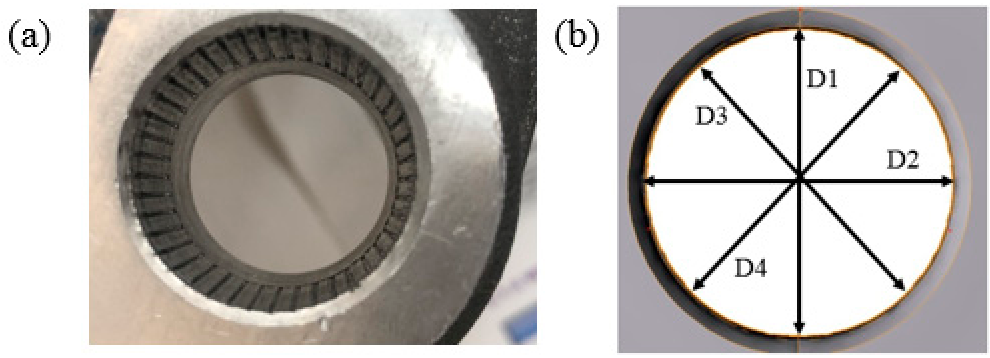

Figure 12. Hoop deformation measurement (in mm): (**a**) schematic hub of the experiment and (**b**) schematic hub of the simulation.

Table 6. Hoop deformation results with hub thicknesses of 10 and 15 mm in method A.

COF \ POS	D1	D2	D3	D4
10 mm				
0.45	24.17	24.22	23.48	23.50
0.61	23.75	23.29	23.40	23.80
0.7	23.55	23.65	23.39	23.39
0.8	23.48	24.00	23.50	24.0
AVG	23.73	23.79	23.44	23.67
15 mm				
COF \ POS	**D1**	**D2**	**D3**	**D4**
0.45	24.82	23.51	23.47	23.34
0.61	24.19	24.04	23.71	23.49
0.7	23.61	23.48	23.43	23.43
0.8	23.63	24.45	24.00	23.35
AVG	24.06	23.87	23.65	23.40

Table 7. Hoop deformation results with hub thicknesses of 10 and 15 mm in method B.

COF \ POS	D1	D2	D3	D4
10 mm				
0.45	23.60	23.68	23.86	23.61
0.61	23.45	23.47	23.55	23.63
0.7	23.44	23.47	23.55	23.63
0.8	23.38	23.48	23.92	24.26
AVG	23.46	23.52	23.72	23.78
15 mm				
COF \ POS	**D1**	**D2**	**D3**	**D4**
0.45	23.47	23.61	23.79	23.40
0.61	23.51	23.31	23.66	23.31
0.7	23.39	23.31	23.39	23.22
0.8	23.67	23.56	23.63	23.52
AVG	23.51	23.44	23.61	23.46

For the jointing process, two shaft chamfer angles were used, as shown in Figure 13. A large chamfer angle causes higher forming force values as mentioned above, and the dimension of the chamfer angle also influences the joining force during the jointing process. Results of a comparison between the two simulation methods are shown in Figure 13a,b. The forming surface of the method B simulations provided more clear texture than in method A, which means that the arrangement of the mesh size in method B is more precise than in method A (Figure 13b). Theoretically, the effective stress at the groove of the hub surface with different COF values between methods A or B showed almost the same trend. The maximum effective stress was about 330 MPa.

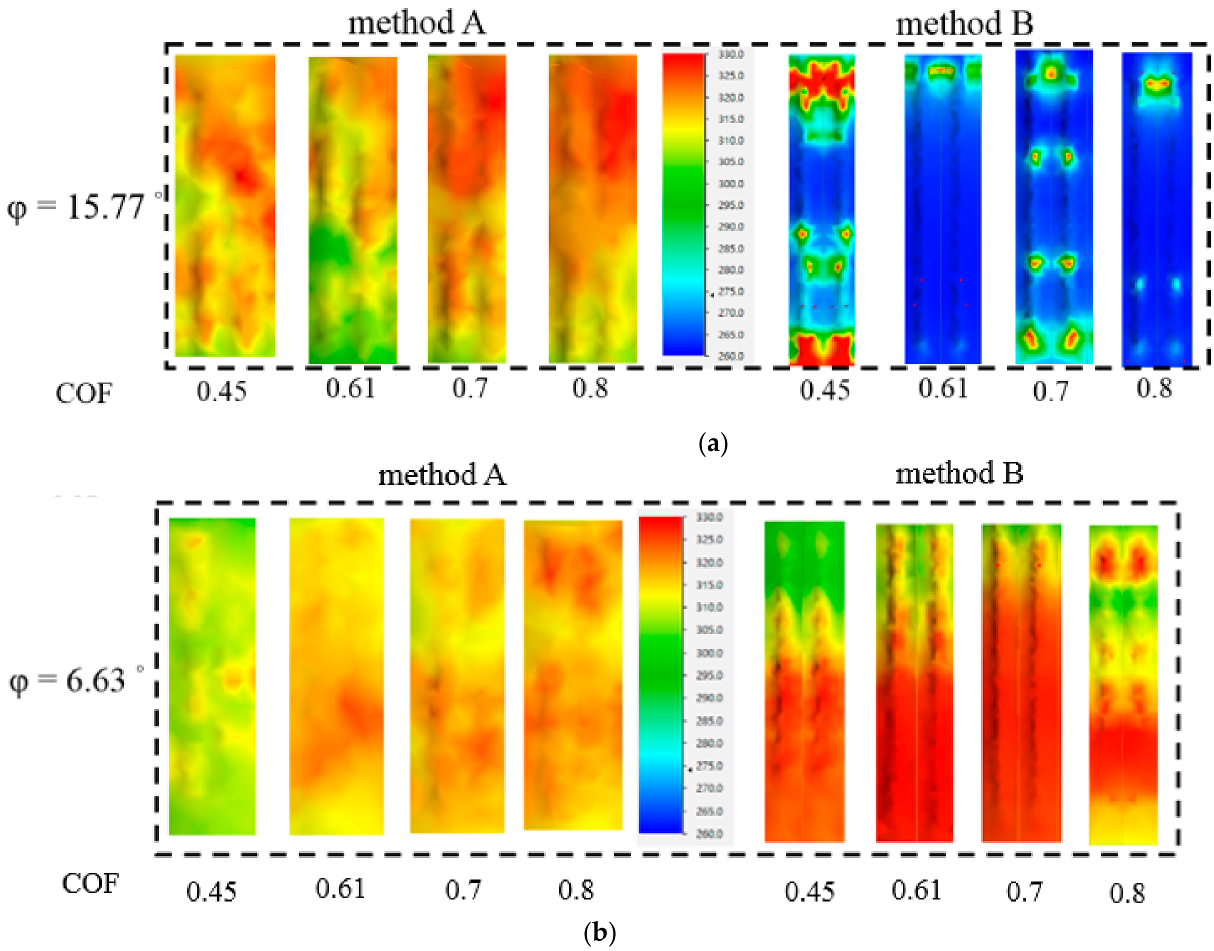

Figure 13. Effective stress at the groove of the hub surface with different COF values: (**a**) shaft angle of 15.77° and (**b**) shaft angle of 6.63°.

4. Results and Discussion

Although this study only conducted a brief analysis and experiment on the surface texture of the hub, it provided three different versions of the shaft with a numerical analysis of finite element models in the jointing process. Simulation values for the process design parameters include shaft chamfer angle, shaft diameter, COF, and hub thickness. The best coefficient of friction value was determined by the simulation and experiment in this study. Additionally, the research on jointing force found that the COF value is directly proportional to the jointing force value and has no correlation with hub thickness. The thickness of the hub and the simulation method have simultaneously little effect on hoop deformation. If the COF value is too high, the joining force can easily become too large, meaning a moderate COF value should be selected.

On the other hand, the error and accuracy of the simulated jointing force of method B were better than those of method A, the forming surface of the method B simulations provided more clear texture than in method A, and the best simulation method was selected between the two simulation methods. Through the study of the jointing force, it was demonstrated that the shaft design of version 3 was the best combination of process parameters. Finally, the enlarged view of the geometry of the contact region between the shaft and the hub illustrated the extremely high numerical similarity of the experimental and simulated cross-sectional shapes of the gear.

5. Conclusions

In this study, the hub thickness and jointing force, shaft design parameters, simulation method differences, and COF numerical correlation were researched, and conclusions were obtained. In the future, further research will be conducted on the surface texture of the hub or the fatigue life of the hub. Therefore, the research results of the knurled interference fit of this article can be summarized as follows:

1. The average deviations of the two finite element simulation methods proposed in this study were less than ±5% in the jointing force in comparison with the experiment, indicating that the finite element method can be accurately applied in the experimental analysis of KIF.
2. According to the statistics of the jointing force data and the hoop deformation analysis, the thickness of the hub has little effect on the KIF jointing force and hoop dimension; there is no absolute correlation between the two.
3. The shaft design of version 3 had the lowest jointing force (156~158 KN) and the smallest error in the simulated and experimental data, meaning version 3 was the best shaft design in this study. The shaft design of version 3 has a smaller chamfer angle (6.63°) than the shaft design of version 1, which can reduce the KIF engagement force and manufacturing cost.
4. According to the comparative analysis of the jointing force and the tooth profile of different shaft designs, the error between the jointing force of the simulation and the experimental value was smallest in method B (mean ratio of joining force accuracy was more than 97%), and the average value of the tooth profile difference was higher (average height accuracy was more than 99%), which means simulation method B should be selected as the best simulation method. The results show that in the finite element simulation method, for the analysis of small deformation, the mesh size in simulation analysis will greatly affect the accuracy of the analysis results.
5. By comparing the jointing force values of different shaft designs, it was found that the jointing force was proportional to the COF value. Therefore, to improve the torque force of the KIF structure, process conditions with a larger COF value should be selected. However, if the COF value is too high, it is easy to cause an excessive jointing force and increase the manufacturing cost. Therefore, a moderate COF value should be selected. A COF of 0.61 is the best friction coefficient value observed in this study.

Author Contributions: Conceptualization, C.-P.C.; methodology, C.-P.C.; software, M.H.; validation, C.-P.C. and M.H.; formal analysis, C.-P.C.; investigation, C.-P.C. and Y.-K.F.; resources, Y.-K.F. and M.H.; data curation, C.-P.C.; writing—original draft preparation, C.-P.C.; writing—review and editing, C.-P.C., T.-T.L. and Y.-K.F.; visualization, C.-P.C.; supervision, T.-T.L. and Y.-K.F.; project administration, M.H. All authors have read and agreed to the published version of the manuscript.

Funding: This research received no external funding.

Institutional Review Board Statement: All authors have no comments for the Institutional Review Board.

Informed Consent Statement: All authors consent to publish this article with its included data in *Metals* and approve its final version.

Data Availability Statement: The authors confirm that the data supporting the findings of this study are available within the article.

Conflicts of Interest: The authors declare no conflict of interest.

References

1. Deng, L.; Xia, J.; Wang, X. *Precision Forging Technology and Equipment for Aluminum Alloy*, 1st ed.; The Gateway; Springer: Singapore, 2022; pp. 11–40.
2. Panwar, N.; Chauhan, A.; Pali, H.S.; Sharma, M.D. Fabrication of aluminum 6061 red-mud composite using stir casting and micro structure observation. *Mater. Today Proc.* **2020**, *21*, 2014–2023. [CrossRef]
3. Lee, I.K.; Lee, S.Y.; Lee, S.K.; Jeong, M.S.; Kim, B.J.; Joo, W.G. Study on effect of shapes of serration of joining plane on joining characteristics for the aluminum–steel multi-materials press joining process. *Materials* **2020**, *13*, 5611. [CrossRef] [PubMed]
4. Raj, A.P.; Bhatti, A.; Dhanish, P.B. Combined effect of cylindricity, roundness and roughness on axial load-carrying ability of interference fits. *Proc. Inst. Mech. Eng. Part J.-J. Eng. Tribol.* **2020**, *234*, 1697–1711. [CrossRef]
5. Sohrabpoor, H.; Mousavian, R.T.; O'Halloran, S.; Benyounis, K.Y.; Baraheni, M.; Obeidi, M.A.; Ahad, I.U.; Raghavendra, R.; Brabazon, D. Experimental and empirical model analysis of microsurface texturing on 316 L press-fit joints fabricated by selective laser melting. *J. Adv. Manuf. Technol.* **2020**, *108*, 2687–2699. [CrossRef]
6. Lü, X.; Zhao, J.; Hu, L.; Wang, H. Effect of interference fits on the fatigue lives of bolted composite joints. *J. Shanghai Jiaotong Univ. Sci.* **2016**, *21*, 648–654. [CrossRef]
7. Romanov, A.V.; Shchenyatsky, A.V.; Petrov, A.V. Hydropress assembling automation of interference fits with steel and titanium parts. *IOP Conf. Ser. Mater. Sci. Eng.* **2020**, *971*, 042064. [CrossRef]
8. Obeidi, M.A.; McCarthy, E.; Brabazon, D. Methodology of laser processing for precise control of surface micro-topology. *Surf. Coat. Technol.* **2016**, *307*, 702–712. [CrossRef]
9. Hirot, K.; Kitamura, K.; Ukai, Y.; Matsunaga, K. Mechanical joining of shaft and holed disc in rotational and axial directions. *Procedia Eng.* **2017**, *207*, 980–985. [CrossRef]
10. McMillan, M.D.; Booker, J.D.; Smith, D.J.; Onisa, C.F.; Korsunsky, A.M.; Song, X.; Baimpas, N.; Evans, A. Analysis of increasing torque with recurrent slip in interference-fits. *Eng. Fail. Anal.* **2016**, *62*, 58–74. [CrossRef]
11. Wang, Y.; Lee, S.H. Design and analysis on interference fit in the hardwood dowel-glued Joint by finite element method. *Procedia Eng.* **2014**, *79*, 166–172. [CrossRef]
12. Jin, J.S.; Xia, J.C.; Wang, X.Y.; Hu, G.A.; Liu, H. Die design for cold precision forging of bevel gear based on finite element method. *J. Cent. South Univ. Technol.* **2009**, *16*, 546–551. [CrossRef]
13. Seifi, R.; Abbasi, K. Friction coefficient estimation in shaft/bush interference using finite element model updating. *Eng. Fail. Anal.* **2015**, *57*, 310–322. [CrossRef]
14. Lou, Z.; Wang, X.; Wang, Y.; Wang, X.; Xu, C.; Wang, Z. Precision assembly method of a kind of small interference fitting parts. *Sādhanā* **2019**, *44*, 144. [CrossRef]
15. Wang, X.; Lou, Z.; Wang, X.; Xu, C. A new analytical method for press-fit curve prediction of interference fitting parts. *J. Mater. Process. Technol.* **2017**, *250*, 16–24. [CrossRef]
16. Zhang, P.; Kou, S.; Lin, B.; Wang, Y. Optimization for radial knurling connection process of assembled camshaft using response surface method. *J. Adv. Manuf. Technol.* **2014**, *77*, 653–661. [CrossRef]
17. Lanoue, F.; Vadean, A.; Sanschagrin, B. Finite element analysis and contact modelling considerations of interference fits for fretting fatigue strength calculations. *Simul. Model. Pract. Theory* **2009**, *17*, 1587–1602. [CrossRef]
18. Izard, E.; Garcia, R.; Manuel, R.M.; Lorenzo, M. Finite element analysis of the reduction in stress concentration factors in shrink fits by using contact rings. *Appl. Sci.* **2022**, *12*, 10037. [CrossRef]
19. Brake and Front End. Available online: https://www.brakeandfrontend.com/complete-wheel-bearing-service/ (accessed on 30 October 2022).
20. Kleditzsch, S.; Awiszus, B.; Lätzer, M.; Leidich, E. Numerical and analytical investigation of steel–aluminum knurled interference fits: Joining process and load characteristics. *J. Mater. Process. Technol.* **2015**, *219*, 286–294. [CrossRef]
21. Ludwik, P. *Elemente der Technologischen Mechanik*, 1st ed.; Springer: Berlin/Heidelberg, Germany, 1909; pp. 11–35.
22. SEYI. Available online: https://zh-tw.seyi.com/index.php?s=spec_search&c=search901 (accessed on 30 October 2022).